CHAPTER VI
HYDROGEN PRODUCTION OVER METAL-LOADED MESOPOROUS-ASSEMBLED $SrTiO_3$ NANOCRYSTAL PHOTOCATALYSTS: EFFECTS OF METAL TYPE AND LOADING

Abstract

Mesoporous-assembled $SrTiO_3$ photocatalysts with different loaded metal co-catalysts (Au, Pt, Ag, Ni, Ce, and Fe) synthesized by the single-step sol-gel method with the aid of a structure-directing surfactant were tested for the photocatalytic activity of hydrogen production from a methanol aqueous solution under both UV and visible light irradiation. The Au, Pt, Ag, and Ni loadings had a positive effect on the photocatalytic activity enhancement, whereas the Ce and Fe loadings did not. The best loaded metal was found to be Au due to its electrochemical properties compatible with the $SrTiO_3$-based photocatalyst and its visible light harvesting enhancement. A 1 wt.% Au-loaded $SrTiO_3$ photocatalyst exhibited the highest photocatalytic hydrogen production activity with a hydrogen production rate of 337 and 200 $\mu mol\ h^{-1}\ g_{cat}^{-1}$ under UV and visible light irradiation, respectively. The hydrogen diffusivity from the liquid phase to the gas phase also significantly affected the photocatalytic hydrogen production efficiency. An increase in the hydrogen diffusability led to an increase in the photocatalytic hydrogen production efficiency.

6.1 Introduction

For hydrogen production from the photocatalytic water splitting reaction, the three main reasons for the low hydrogen production activity of most photocatalysts are the high recombination rate between the photo-generated electron and hole [1], the fast backward reaction between hydrogen and oxygen into water [2-8], and the limited light harvesting ability of the photocatalysts themselves [3,9-11]. Hence, several research projects have focused on eliminating these obstacles and enhancing the visible light harvesting ability of the photocatalysts [12-20]. One interesting approach used for enhancement of the photocatalytic activity of hydrogen

To be published in International Journal of Hydrogen Energy, 35 (2010) 6531-6540

evolution by increasing the charge transfer to reduce the recombination rate is to load a metal catalyst, or co-catalyst. The loaded metal, or co-catalyst, can act as a charge transferring site and/or active site for the photocatalytic reaction. It has been reported that the photocatalytic activity of TiO_2 can be remarkably enhanced by the loading of a small amount of a Pt co-catalyst [21-27]. The enhancement in the photocatalytic activity can be explained by the photoelectrochemical mechanism, in which the photo-generated electrons quickly migrate to the Pt particles loaded on the TiO_2 surface, where the proton reduction reaction proceeds. In this case, Pt behaves as both charge transferring and active sites [28]. The use of NiO as the co-catalyst for improving the photocatalytic hydrogen production activity of both the mesoporous TiO_2 and Ta_2O_5 photocatalysts was elucidated experimentally [29,30]. $SrTiO_3$ photocatalysts also showed photocatalytic hydrogen production capability, and its photocatalytic hydrogen production activity was significantly enhanced by loading NiO [31]. A Cr-Ta-doped $SrTiO_3$ photocatalyst showed photocatalytic hydrogen production activity under visible light irradiation, and its photocatalytic activity was drastically increased with Pt loading [32]. The influence of a CoO co-catalyst on the photocatalytic activity of La-doped $SrTiO_3$ was also studied, and the increase in the photocatalytic activity was due to the role of the loaded CoO, which can capture the electrons from the n-type semiconductor $SrTiO_3$, resulting in recombination prevention [33]. However, to update information, the comparative investigation for photocatalytic hydrogen production of mesoporous-assembled $SrTiO_3$ photocatalyst with various loaded metal co-catalysts has not yet been performed.

In our previous work, mesoporous-assembled perovskite-type $SrTiO_3$ photocatalysts were tested for their photocatalytic activity via the photocatalytic methyl orange degradation [34] and the photocatalytic hydrogen production from water using methanol as a sacrificial reagent [35]. The results indicated that the mesoporous-assembled structure of $SrTiO_3$ nanocrystals is responsible for the enhancement of the photocatalytic activity of the $SrTiO_3$ photocatalyst, exhibiting much higher photocatalytic activities than the commercially available non-mesoporous-assembled $SrTiO_3$ and TiO_2 nanopowders (i.e. Wako $SrTiO_3$ and Degussa P-25 TiO_2). Due to the high ability of the $SrTiO_3$ photocatalyst to produce hydrogen from water [10,11,31,36,37], this present work focused on further

enhancement of the photocatalytic hydrogen production activity by modifying the mesoporous-assembled $SrTiO_3$ photocatalyst by the metal co-catalyst loading via the single-step sol-gel method. Although some loaded co-catalysts may be buried inside the photocatalyst matrix, the single-step sol-gel method was selected for synthesizing the co-catalyst-loaded mesoporous-assembled $SrTiO_3$ due to its several advantages: (1) it is a more straightforward method for loading a metal co-catalyst than the conventional methods (e.g. incipient wetness impregnation), which require two separate steps of support preparation and co-catalyst loading, (2) based on our previous experience, it provides a high dispersion of a loaded co-catalyst in the resulting photocatalyst, and (3) the interaction between the base photocatalyst and the loaded co-catalyst becomes greater, resulting in a higher photocatalytic activity of the loaded photocatalyst prepared by this method as compared to the conventional methods [21,29,35]. The present results clearly revealed, for the first time, that the mesoporous-assembled $SrTiO_3$ with the Au co-catalyst exhibited the highest photocatalytic hydrogen production activity, as compared to the other studied loaded metal co-catalysts. In addition, the photocatalytic hydrogen production activity of the mesoporous-assembled $SrtiO_3$ with an optimum Au loading was also enhanced by adjusting operational parameters of the photocatalytic system.

6.2 Experimental

6.2.1 Materials

Strontium nitrate ($Sr(NO_3)_2$, Merck Co., Ltd.), tetraisopropyl orthotitanate (TIPT, Merck Co., Ltd.), acetylacetone (ACA, S.D. Fine-Chem Ltd.), laurylamine (LA, Merck Co., Ltd.), hydrochloric acid (HCl, 37% analytical grade, Labscan Asia Co., Ltd.), and anhydrous ethanol (EtOH, Italmar Co., Ltd.) were used as starting materials for the mesoporous-assembled $SrTiO_3$ nanocrystal photocatalyst synthesis. Hydrogen tetrachloroaurate (III) trihydrate ($HAuCl_4 \cdot 3H_2O$, Alfa Aesar), hydrogen hexachloroplatinate (IV) hexahydrate ($H_2PtCl_6 6H_2O$, Aldrich Co., Ltd.), nickel (II) nitrate hexahydrate ($Ni(NO_3)_2 \cdot 6H_2O$, Wako Pure Chemical Industries, Ltd.), silver nitrate ($AgNO_3$, Nacalai Tesque), iron (III) nitrate nanohydrate

($Fe(NO_3)_3 \cdot 9H_2O$, Wako Pure Chemical Industries, Ltd.), and cerium (IV) di-ammonium nitrate ($(NH_4)_2Ce(NO_3)_6$, Chamelean Reagent) were used as Au, Pt, Ni, Ag, Fe, and Ce co-catalyst precursors, respectively. Anhydrous methanol (MeOH, Labscan Asia Co., Ltd.) was used as a sacrificial reagent, acting as a hole scavenger, for the investigation of the photocatalytic hydrogen production activity.

6.2.2 Synthesis Procedure of Mesoporous-Assembled $SrTiO_3$ Photocatalysts

The mesoporous-assembled $SrTiO_3$ nanocrystal photocatalysts, without and with different metal types and loadings, were synthesized via the sol-gel process with the aid of a structure-directing surfactant under mild conditions [34,35]. ACA was first added to TIPT at an equimolar proportion. A laurylamine hydrochloride (LAHC) solution was prepared by dissolving LA with an equimolar HCl in 50 cm^3 of EtOH, based on the LAHC-to-TIPT molar ratio of 0.25:1. Then, a specified amount of $Sr(NO_3)_2$, based on the Sr-to-Ti molar ratio of 1:1, was added to the LAHC solution with continuous stirring to obtain a clear solution. For the metal-loaded mesoporous-assembled $SrTiO_3$ nanocrystal photocatalysts synthesized via the single-step sol-gel method, each metal of various amounts was added to this clear solution to obtain various loadings, being analogous to the Pt- and Ni-loaded mesoporous-assembled TiO_2 [21,29]. Afterwards, the LAHC/$Sr(NO_3)_2$ or LAHC/$Sr(NO_3)_2$/metal solution was slowly dropped into the TIPT/ACA solution while stirring continuously. The resultant mixture was incubated at 80°C for 1 d to obtain complete gel formation. The resulting gel was further dried at 80°C for 2 d. Finally, the dried gel was calcined at 700°C for 4 h, which were found to be the optimum calcination conditions in our previous work [34], to yield the mesoporous-assembled $SrTiO_3$ nanocrystal photocatalysts (pristine $SrTiO_3$) or the metal-loaded mesoporous-assembled $SrTiO_3$ nanocrystal photocatalysts (metal-loaded $SrTiO_3$).

6.2.3 Photocatalyst Characterization Techniques

The crystallinity and the purity of the pristine and metal-loaded $SrTiO_3$ photocatalysts were examined by X-ray diffraction (XRD, Rigaku, RINT-

2100) with a rotating anode XRD generating monochromated CuK_α radiation using continuous scanning mode at a rate of 2°C min^{-1} and operating conditions of 40 kV and 40 mA. The $SrTiO_3$ crystallite size (D) was calculated from the line broadening of the $SrTiO_3$ (110) diffraction peak by using the Debye-Scherrer equation [38]:

$$D = \frac{K\lambda}{\beta\cos(\theta)}$$

where K is the Scherrer constant (0.89), λ is the wavelength of the X-ray radiation (0.15418 nm for CuK_α), β is the full width half maximum (FWHM) of the diffraction peak measured at 2θ, and θ is the diffraction angle.

The actual metal loading of the synthesized $SrTiO_3$ photocatalysts was analyzed by X-ray fluorescence spectroscopy (XRF, Phillip, WD-XRF model PW-2400). The N_2 adsorption–desorption isotherms of the synthesized $SrTiO_3$ photocatalysts were obtained by using a nitrogen adsorption–desorption apparatus (BEL Japan, BELSORP-18 PLUS) at a liquid nitrogen temperature of -196°C. The specific surface areas of the synthesized $SrTiO_3$ photocatalysts were determined by the Brunauer-Emmett-Teller (BET) approach using the adsorption data. Mean pore size and pore size distribution were determined by the Barrett-Joyner-Halenda (BJH) approach using the desorption data. Diffuse reflectance spectra of the synthesized $SrTiO_3$ photocatalysts were obtained by using a UV-visible spectrophotometer (Shimadzu, UV-2450) at room temperature with $BaSO_4$ as the reference. Afterwards, the diffuse reflectance spectra were analyzed to estimate the band gap wavelength (λ_g, nm) by using the Kabelka–Munk function, and the band gap energy (E_g) was then determined by using the following equation [39]:

$$E_g = \frac{1240}{\lambda_g}.$$

6.2.4 Photocatalytic Hydrogen Production System

The photocatalytic hydrogen production activity of the pristine and the metal-loaded $SrTiO_3$ photocatalysts was investigated by using the rate of hydrogen production during a 5-h irradiation period as a process performance parameter. The photocatalytic experiments were performed in an outer-irradiation

and air-tight Pyrex glass reactor with a total volume of 750 cm^3. The reaction temperature was controlled by using a water-cooling system. A set of 176 W Hg lamps (Phillip Co. Ltd.), which emitted light of more than 95% with a wavelength of 254 nm and with total irradiating intensity of 2.3 mW cm^{-2}, and a 300 W Xe lamp (KXL-300, Wacom Electric) combined with a UV cutoff filter (ATG, B-485), which allowed only the visible light with wavelengths longer than 400 nm to pass with total irradiating intensity of 2.6 mW cm^{-2}, were employed as UV and visible light sources, respectively. In a typical experiment, each photocatalyst sample was suspended in a 50 vol.% methanol aqueous solution, which was found to be the most suitable concentration in our previous work [35], by using a magnetic stirrer. Prior to the reaction testing, the suspension was left in the dark while simultaneously being thoroughly deaerated by Ar gas bubbling for 20 min, and then the suspension was irradiated by turning on the lamps for 5 h. For the UV irradiation, the liquid phase volume was controlled at 500 cm^3 (except for the experiment to determine the effect of the gas phase-to-liquid phase volumetric ratio), and the reaction temperature was controlled at 45°C, which was found to be the most suitable reaction temperature [35]. For the visible light irradiation, the liquid phase volume was controlled at 200 cm^3, and the reaction was performed at room temperature. A gas sample in the headspace of the studied reactor was periodically withdrawn at 1 h intervals and analyzed for hydrogen concentration by using a gas chromatograph (Hayesep D100/120, PerkinElmer) equipped with a thermal conductivity detector (TCD). The control experiments using the synthesized photocatalysts in the dark showed no hydrogen production from the methanol aqueous solution under both the UV and the visible light irradiation. The effects of photocatalyst dosage and gas phase-to-liquid phase volumetric ratio on the photocatalytic hydrogen production activity were also investigated over the best metal-loaded $SrTiO_3$ photocatalyst.

6.3 Results and discussion

6.3.1 Characterization Results

All XRD patterns of the pristine and the metal-loaded $SrTiO_3$ photocatalysts exemplified in Figure 6.1 (for 0.5 wt.% metal loading) exhibit the

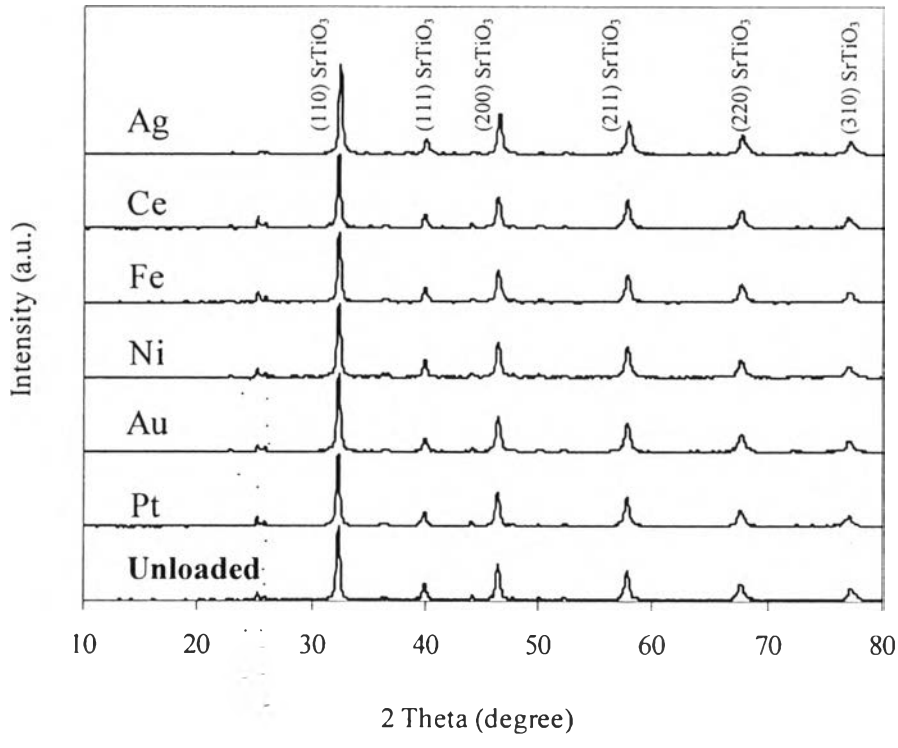

Figure 6.1 XRD patterns of the pristine and the 0.5 wt.% metal-loaded $SrTiO_3$ photocatalysts.

same dominant peaks, which refers to the single phase of cubic perovskite-type $SrTiO_3$, with similar intensity, indicating that all the loaded metals at low loadings in the investigated range of 0.1–1.5 wt.% do not significantly affect the crystallinity and purity of the synthesized $SrTiO_3$ photocatalysts, as well as the $SrTiO_3$ crystallite size (Table 6.1). No crystalline phases of the metals loaded via the single-step sol-gel method were observed in the XRD patterns, probably due to their high dispersion through the mesoporous-assembled structures. However, based on our previous experiences, the phases of Au, Pt, Ag, Ni, Ce, and Fe in the final products are in the forms of metallic Au [40], metallic Pt [21,35], metallic Ag [41], NiO [29,30], CeO_2 [42], and Fe_2O_3 [43] after the calcination step of the metal-loaded dried gels. These original forms of metals were instantaneously used for the photocatalytic investigation without any further reduction step in order to verify the intrinsic advantage of the single-step sol-gel technique for photocatalyst synthesis.

The actual metal loadings of the synthesized $SrTiO_3$ photocatalysts obtained from XRF were not significantly different from the nominal metal loadings (Table 6.1). This implies that the single-step sol-gel method used for loading metals is reliably effective in controlling any desired co-catalyst loading. The light-harvesting ability of all the synthesized $SrTiO_3$ photocatalysts were determined from their UV-visible absorption spectra. The results show that the presence of each loaded metal in the mesoporous-assembled $SrTiO_3$ nanocrystal photocatalyst greatly contributes to the increase in the light-harvesting ability within the visible region ($\lambda > 400$ nm), as shown in Figure 6.2. Particularly, the addition of either Au or Ni significantly enhanced the visible light-harvesting ability up to a wavelength of 800 nm. Moreover, each loaded metal accordingly affected the band gap energy of the synthesized $SrTiO_3$ photocatalysts, as shown in Table 6.1. It can be seen that in general, the band gap energy of the synthesized $SrTiO_3$ photocatalysts decreased in the presence of loaded metals because of the increase in the absorption onset wavelength.

The type IV IUPAC pattern with a distinct hysteresis loop of the N_2 adsorption–desorption isotherms of all the synthesized $SrTiO_3$ photocatalysts (Figure 3) indicates their mesoporous structure with very narrow pore size distributions (insets of Figure 6.3), originating from the assembly of $SrTiO_3$ nanocrystals [34,35]. Under the synthesis conditions, the results suggest that the loading with various metals does not greatly affect the mesoporous-assembled structure of the synthesized $SrTiO_3$ photocatalysts. Moreover, the N_2 adsorption–desorption analysis results showed that although a higher metal loading tends to slightly decrease the specific surface area, mean pore diameter, and total pore volume, none of the loaded metals significantly affect these textural characteristics of the synthesized $SrTiO_3$ photocatalysts, as shown in Table 6.1, with the specific surface area in the range of 8–12 m^2/g, mean pore diameter in the range of 4.2–4.8 nm, and total pore volume in the range of 64–85 mm^3/g.

Table 6.1 Textural properties of all studied photocatalysts from XRF, XRD, UV-visible spectroscopy, and N_2 adsorption–desorption analyses

Photocatalyst	Nominal metal loading (wt.%)	Actual metal loading[a] (wt.%)	Crystallite size of $SrTiO_3$[b] (nm)	E_g[c] (eV)	BET surface area[d] (m^2g^{-1})	Mean pore diameter[d] (nm)	Total pore volume[d] (mm^3g^{-1})
Pristine $SrTiO_3$	-	-	34.98	3.23	12.24	4.8	85
Au-loaded $SrTiO_3$	0.1	0.11	35.29	3.18	11.96	4.8	82
	0.5	0.47	35.12	3.18	10.5	4.8	78
	1.0	0.98	35.06	3.18	8.64	4.4	74
	1.5	1.49	35.11	3.18	7.87	4.2	71
Pt-loaded $SrTiO_3$	0.1	0.1	35.12	3.16	12.04	4.8	81
	0.5	0.43	35.08	3.16	10.77	4.8	79
	1.0	0.91	34.84	3.16	9.31	4.7	78
	1.5	1.52	35.01	3.16	7.77	4.4	65
Ni-loaded $SrTiO_3$	0.1	0.11	35.27	2.98	12.12	4.8	83
	0.5	0.5	35.31	2.98	10.98	4.7	79
	1.0	0.99	35.12	2.98	9.93	4.4	77
	1.5	1.51	35.1	2.98	8.13	4.5	71
Ag-loaded $SrTiO_3$	0.1	0.09	35.15	3.18	12.1	4.7	82
	0.5	0.51	35.14	3.18	11.65	4.8	82
	1.0	1.05	34.99	3.18	10.08	4.5	79
	1.5	1.48	34.96	3.18	8.12	4.3	72
Ce-loaded $SrTiO_3$	0.5	0.5	35.16	3.18	11.91	4.7	81
	1.0	1.02	35.15	3.18	10.98	4.6	79
	1.5	1.49	34.79	3.18	7.95	4.4	68
Fe-loaded $SrTiO_3$	0.5	0.49	35.04	2.95	11.86	4.7	79
	1.0	0.98	34.99	2.95	7.77	4.5	64

[a]From XRF analysis

[b]From XRD analysis

[c]From UV-visible spectroscopy analysis

[d]From N_2 adsorption–desorption analysis

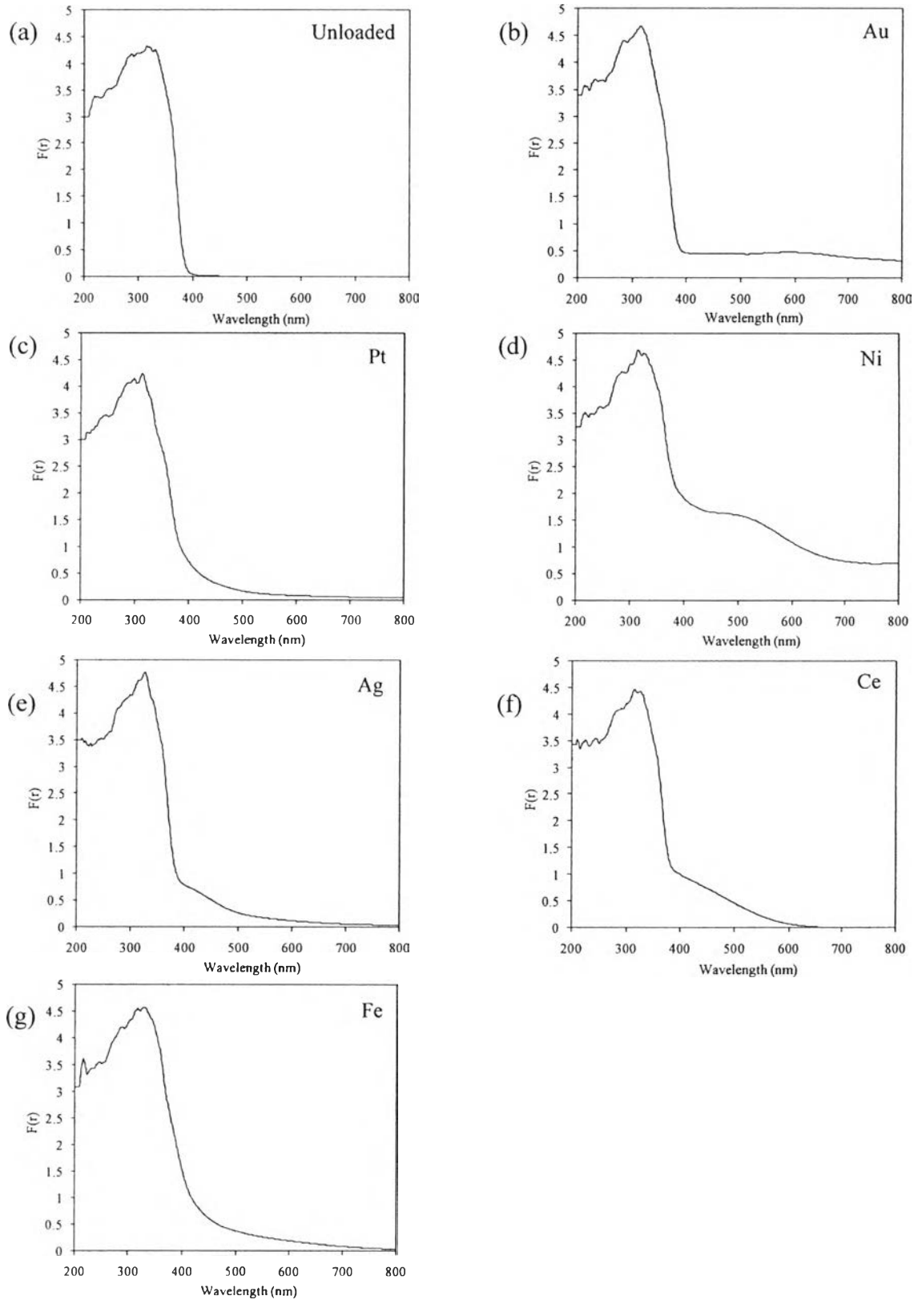

Figure 6.2 Plot of the Kabelka–Munk function (F(r)) as a function of wavelength of the pristine and the 0.5 wt.% metal-loaded $SrTiO_3$ photocatalysts: (a) unloaded, (b) Au, (c) Pt, (d) Ni, (e) Ag, (f) Ce, and (g) Fe.

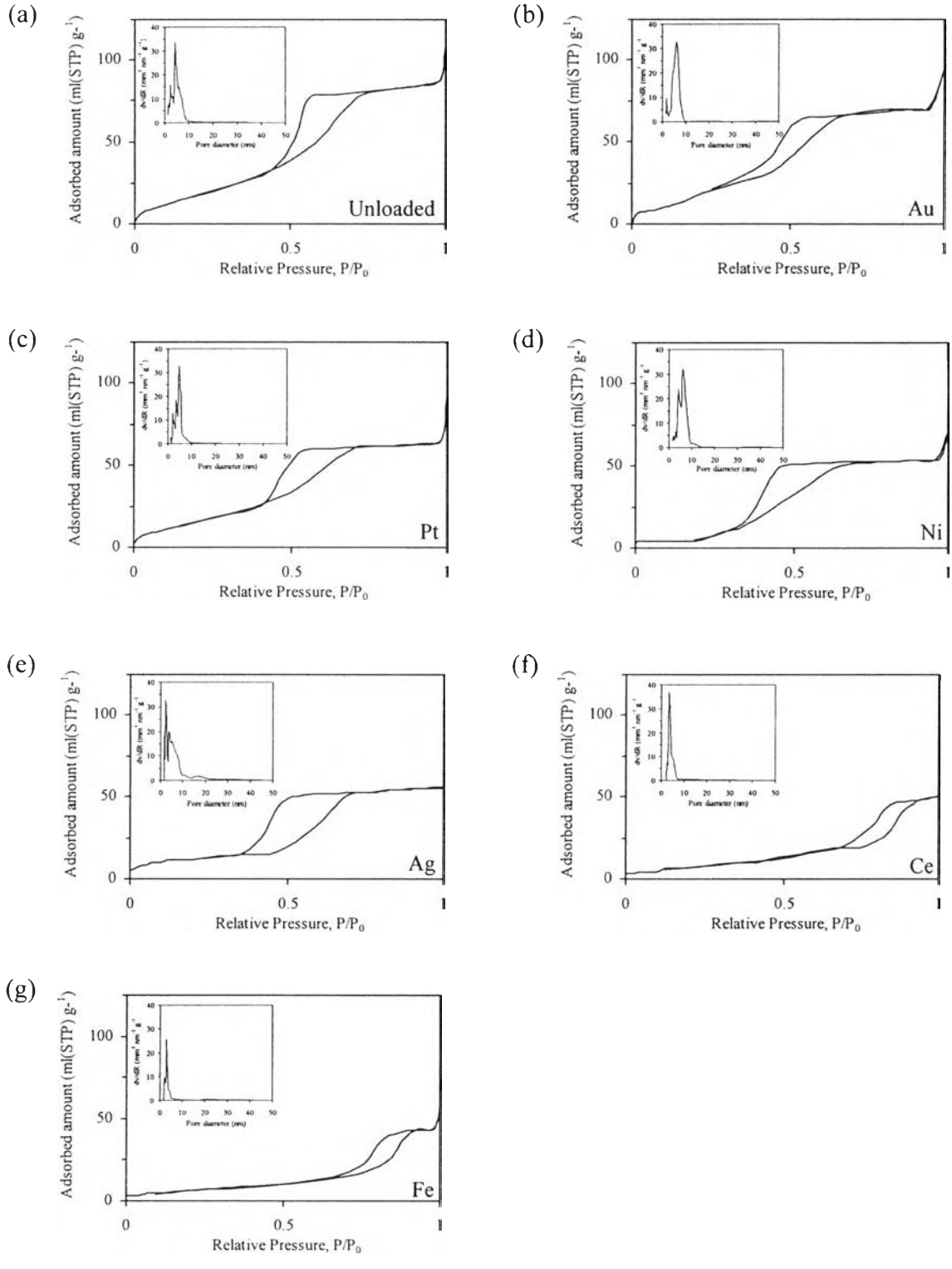

Figure 6.3 N_2 adsorption–desorption isotherms and pore size distributions (inset) of the pristine and the 0.5 wt.% metal-loaded $SrTiO_3$ photocatalysts: (a) unloaded, (b) Au, (c) Pt, (d) Ni, (e) Ag, (f) Ce, and (g) Fe.

6.3.2 Effect of Metal Loading on Hydrogen Production Activity of the $SrTiO_3$-Based Photocatalysts

The hydrogen production activity of the pristine and the metal-loaded $SrTiO_3$ photocatalysts was investigated under both UV and visible light irradiation. The hydrogen production rate for the first 5 h period was used as a comparative indicator of the hydrogen production activity. It should be noted that only hydrogen was detected in the produced gas without detectable carbon dioxide possibly due to its high solubility in water under the studied conditions, and by using a 50 vol.% methanol aqueous solution as a reaction media, the detected hydrogen could be produced mainly from water molecules and partly from methanol (hole scavenger) molecules [35]. For the UV light irradiation system, the results showed that all the Au, Pt, Ni, and Ag loadings had a positive effect on the enhancement of the photocatalytic hydrogen production activity of the pristine $SrTiO_3$ photocatalyst, whereas the Ce and Fe loadings reduced the photocatalytic hydrogen production activity (Figure 6.4(a)). The negative effect of the Ce loading is possibly due to the lower electronegativity of the Ce, as compared to that of Ti, resulting in a more difficult photoexcited electron transfer from a $SrTiO_3$ conduction band to the Ce species. Hence, the Ce possibly behaves as an electron-transfer inhibitor when covering the active sites of the pristine $SrTiO_3$ photocatalyst. For the Fe loading, the Fe also possibly behaves as an inhibitor, similar to the Ce, due to its very low electron affinity, even if its electronegativity is higher than that of Ti [44,45].

The higher electronegativity of all positive-effect loaded metals (Au, Pt, Ni, and Ag) than that of Ti possibly induces them to behave as the active site for proton reduction, resulting in photocatalytic hydrogen production activity enhancement, with the Au-loaded $SrTiO_3$ photocatalyst exhibiting the highest hydrogen production activity (Figure 6.4(a)). According to the electrochemical properties among the positive-effect loaded metals, Au and Pt comparatively have the higher filling orbital level of 5d (4d and 3d for Ag and Ni, respectively) and have the higher electronegativity [44,45]. These possibly lead to the higher photocatalytic hydrogen production activity of the Au- and Pt-loaded $SrTiO_3$ photocatalysts.

(a)

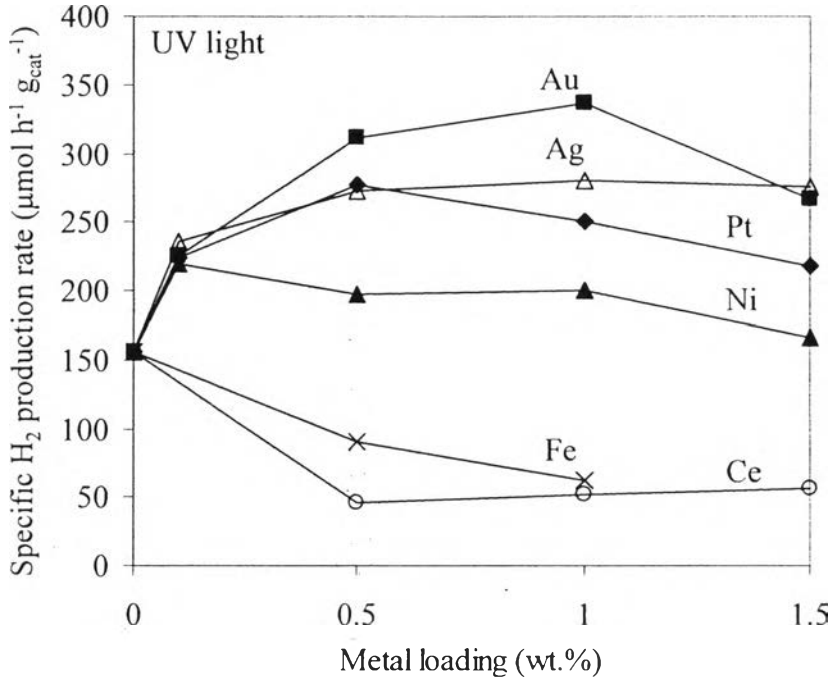

(b)

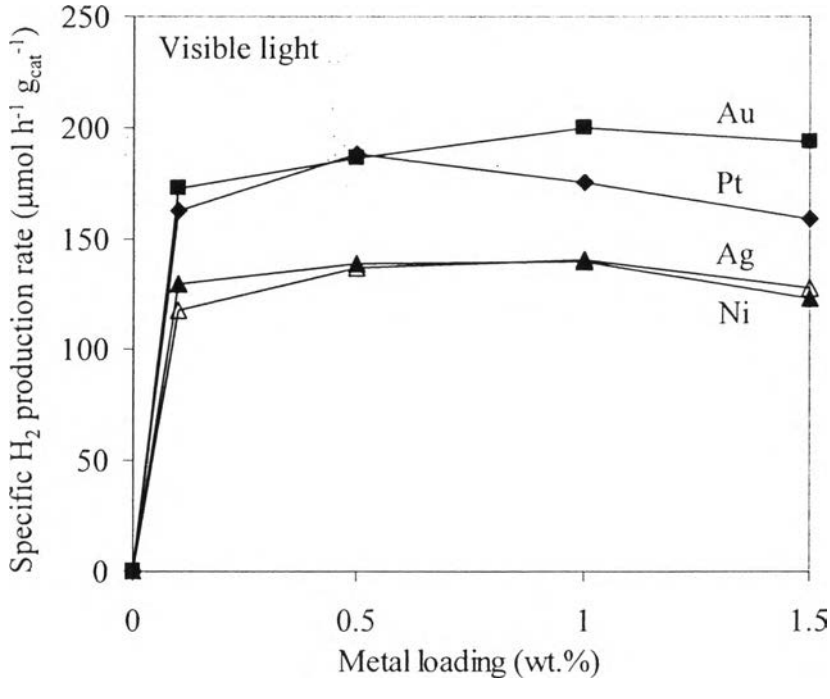

Figure 6.4 Dependence of H_2 production efficiency under (a) UV light irradiation and (b) visible light irradiation on type and quantity of metal loading (system conditions: 5 h irradiation time, 500 (UV) and 200 (visible) cm^3 of a 50 vol.% MeOH aqueous solution, and photocatalyst weight of 0.5 (UV) and 0.2 (visible) g).

In a comparison between Au and Pt, the ionic radius of Au is slightly higher than that of Pt, resulting in a higher H–OH breaking ability [46]. In addition, the higher electronegativity and higher electron affinity of Au as compared to those of Pt [44,45] possibly lead to the highest photocatalytic hydrogen production activity of the Au-loaded $SrTiO_3$ photocatalyst. It can be concluded from the results that the electronegativity of the loaded metal should be higher than that of the base photocatalyst, and its electron affinity should be sufficiently high to maintain the stability of the photogenerated electrons until the proton reduction reaction takes place on the photocatalyst surface.

The increase in the Au loading from 0 to 1 wt.% resulted in an increase in the hydrogen production rate (Figure 6.4(a)). In this Au loading range, the positive effect on the hydrogen production rate was possibly because of the increase in the number of Au active sites with increasing Au loading. However, a further increase in the Au loading higher than 1 wt.% led to a decrease in the hydrogen production rate. This is possibly because the excess Au acts as the electron-hole recombination center, resulting in a negative effect. Therefore, the optimum loading of Au was found to be 1 wt.%, exhibiting the highest hydrogen production rate of 337 μmol h^{-1} g_{cat}^{-1}.

For the visible light irradiation system, the Au-loaded $SrTiO_3$ also exhibited the highest hydrogen production activity (Figure 6.4(b)), and the trend of the Au loading dependence is similar to that occurring in the UV light irradiation system. Even though the Ni-loaded $SrTiO_3$ showed the highest visible-light harvesting ability (Figure 6.2), it exhibited the lowest hydrogen production activity. The results also verify the importance of the electronegativity and the electron affinity of the loaded metals. The highest hydrogen production rate at the optimum Au loading of 1 wt.% under visible light irradiation was 200 μmol h^{-1} g_{cat}^{-1} (Figure 4(b)), which is still lower than that under the UV irradiation condition (337 μmol h^{-1} g_{cat}^{-1}).

6.3.3 Effect of Photocatalyst Dosage

Another way of improving the hydrogen production efficiency is to optimize the operational parameters of this photocatalytic hydrogen production system. In our previous work [35], the effects of reaction temperature, hole scavenger type, and amount of hole scavenger addition were investigated and optimized using a 0.5 wt.% Pt-loaded $SrTiO_3$ photocatalyst. The optimum conditions were found when using MeOH as the hole scavenger, with a MeOH volume fraction of 50 vol.% and a reaction temperature of 45°C. These conditions were further used in the present work to investigate the effects of both the 1 wt.% Au-loaded $SrTiO_3$ photocatalyst dosage and the gas phase-to-liquid phase volumetric ratio on the hydrogen production rate. The effect of the photocatalyst dosage is shown in Figure 6.5(a). The increase in the photocatalyst dosage from 5×10^{-4} to 35×10^{-4} g cm^{-3} results in an increase in the hydrogen production rate. The positive effect on the hydrogen production rate in this photocatalyst dosage range is possibly due to an increase in the total active sites available in the system. However, a further increase in the photocatalyst dosage beyond 35×10^{-4} g cm^{-3} led to a decrease in the hydrogen production rate. With a too high photocatalyst dosage in the system, the light penetration is decreased, leading to a lower quantity of photo-generated electrons. The optimum photocatalyst dosage of 35×10^{-4} g cm^{-3} provided the highest hydrogen production rate of 104 μmol h^{-1}.

Regarding the photocatalyst efficiency in terms of the specific hydrogen production rate (the hydrogen production rate per 1 g of photocatalyst), an increase in the photocatalyst dosage leads to a decrease in the photocatalyst efficiency. This is possibly due to an increase in the H_2 vapor pressure in the gas phase (the fixed gas phase volume of 250 cm^3) when using a higher photocatalyst dosage. In a photocatalytic or catalytic reaction, the product desorption from the photocatalyst/catalyst surface, and the product diffusion, are important mechanisms that directly affect the reaction efficiency [4-7,47].

(a)

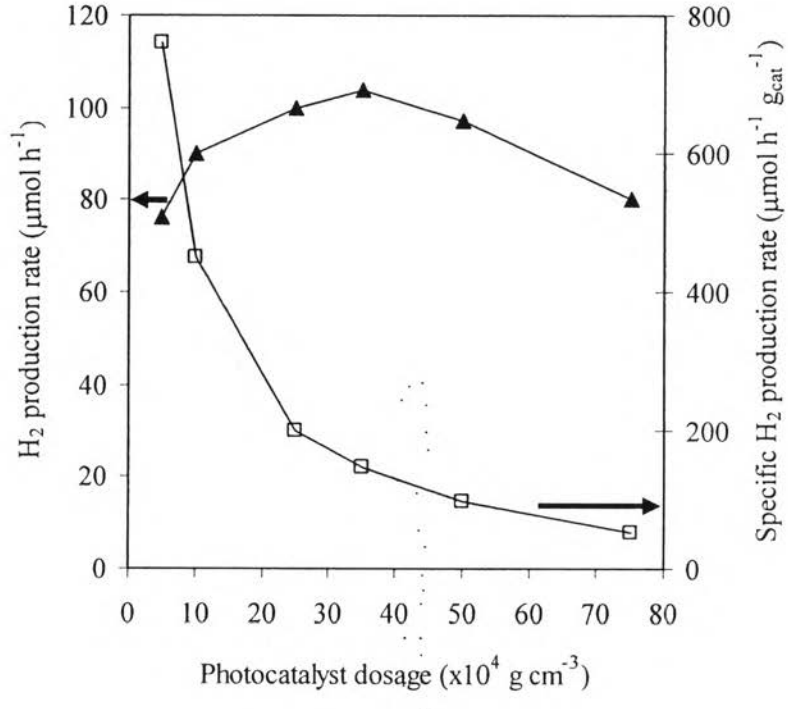

(b)

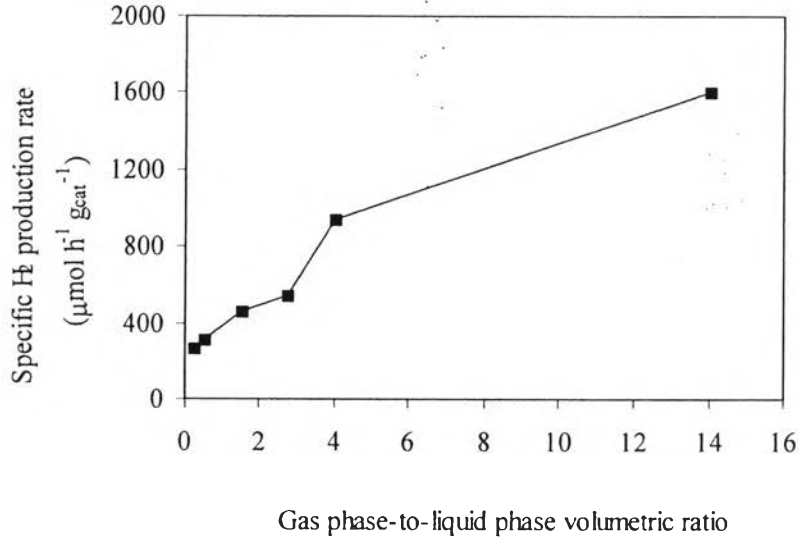

Figure 6.5 Dependence of H_2 production efficiency on (a) photocatalyst dosage (system conditions: 5 h irradiation time, 200 cm^3 of a 50 vol.% MeOH aqueous solution, photocatalyst weight of 0.1-1.5 g, 1 wt.% Au-loaded $SrTiO_3$ photocatalyst, and visible light irradiation) and (b) gas phase-to-liquid phase volumetric ratio (system conditions: 5 h irradiation time, 50 vol.% MeOH aqueous solution, photocatalyst dosage of 1×10^{-3} g cm^{-3}, photocatalyst weight of 0.05-0.6 g, 1 wt.% Au-loaded $SrTiO_3$ photocatalyst, and UV light irradiation).

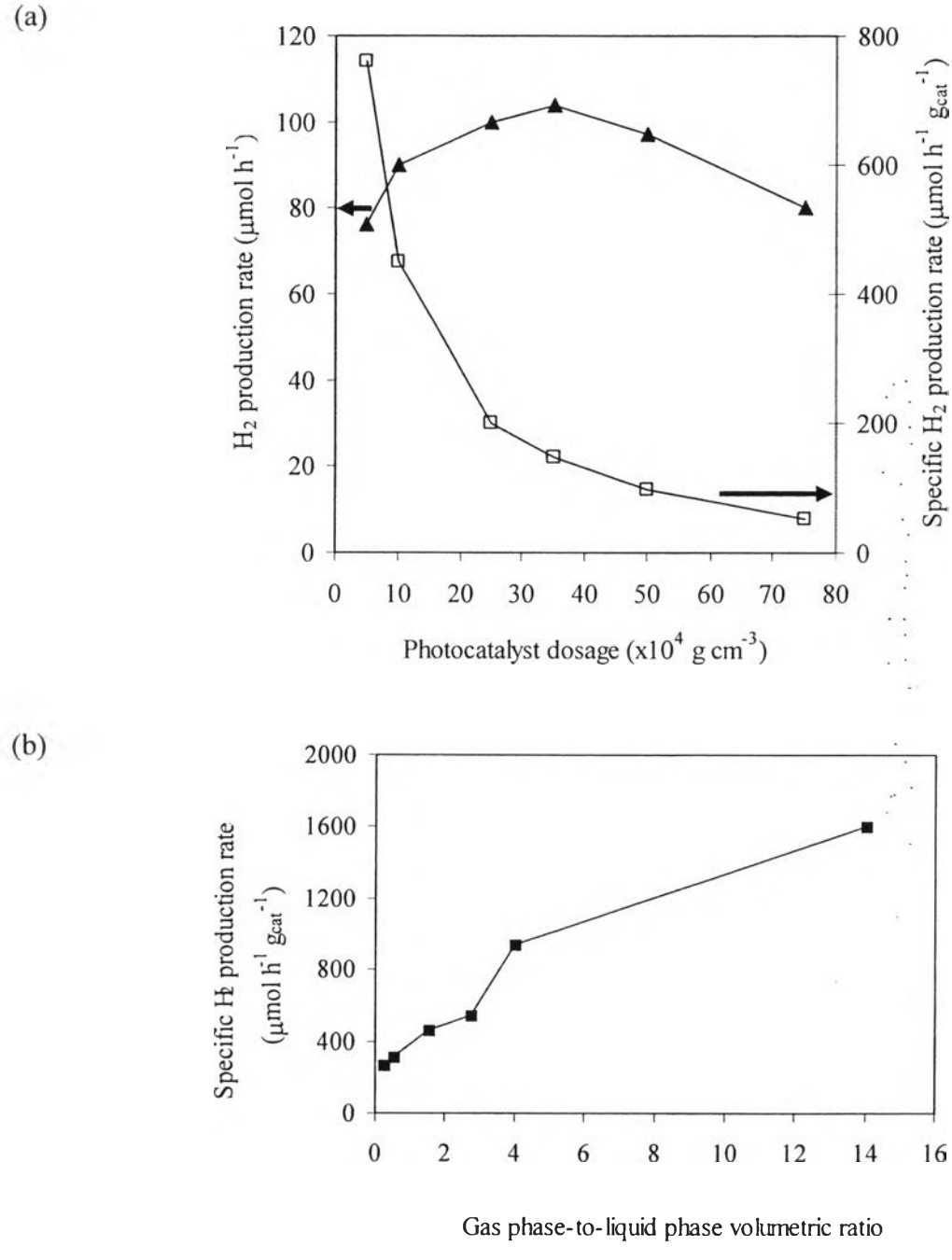

Figure 6.5 Dependence of H_2 production efficiency on (a) photocatalyst dosage (system conditions: 5 h irradiation time, 200 cm^3 of a 50 vol.% MeOH aqueous solution, photocatalyst weight of 0.1-1.5 g, 1 wt.% Au-loaded $SrTiO_3$ photocatalyst, and visible light irradiation) and (b) gas phase-to-liquid phase volumetric ratio (system conditions: 5 h irradiation time, 50 vol.% MeOH aqueous solution, photocatalyst dosage of 1×10^{-3} g cm^{-3}, photocatalyst weight of 0.05-0.6 g, 1 wt.% Au-loaded $SrTiO_3$ photocatalyst, and UV light irradiation).

For this investigated photocatalytic hydrogen production system, an increase in the photocatalyst dosage (referring to the increase in the active sites) provided the higher H_2 evolution and caused a higher H_2 vapor pressure in the gas phase, leading to more difficult H_2 diffusion from the liquid phase to the gas phase. Therefore, the H_2 generated from the photocatalytic reaction remains more in the liquid phase and causes the proton reduction reaction more difficult to proceed, resulting in a decrease in the overall photocatalyst efficiency. This conclusion was also confirmed by the result of the effect of gas phase-to-liquid phase volume ratio, which will be discussed in the next section.

6.3.4 Effect of Gas Phase-to-Liquid Phase Volumetric Ratio

The experiments to investigate the effect of the gas phase-to-liquid phase volumetric ratio were performed by varying the liquid phase volume in the reactor under a constant photocatalyst dosage of 1×10^{-3} g cm^{-3} and a constant gas–liquid interfacial area of 78 cm^2. As shown in Figure 5(b), an increase in the gas phase-to-liquid phase volumetric ratio significantly enhances the specific hydrogen production rate. An increase in the gas phase-to-liquid phase volumetric ratio decreases the H_2 vapor pressure in the system at the same reaction time, resulting in an increase in the probability of H_2 diffusability from the liquid phase to the gas phase, as discussed previously. Hence, the photocatalyst efficiency significantly increases with an increase in the gas phase-to-liquid phase volumetric ratio.

6.4 Conclusions

The metal loading was found to be able to enhance the photocatalytic hydrogen production activity of the mesoporous-assembled $SrTiO_3$ nanocrystal photocatalyst. The characterization results pointed out that the metal loading did not change the physical properties of the synthesized $SrTiO_3$, whereas it did change the light harvesting ability of the pristine mesoporous-assembled $SrTiO_3$ photocatalyst. The enhancement of the photocatalytic hydrogen production activity was found to depend on the electrochemical properties of the loaded metal. Au was found to be the most suitable loaded metal for the hydrogen production over the mesoporous-

assembled $SrTiO_3$-based photocatalyst, exhibiting the highest photocatalytic hydrogen production activity enhancement. An optimum Au loading of 1 wt.% provided the highest hydrogen production rate of 337 μmol h^{-1} g_{cat}^{-1} and 200 μmol h^{-1} g_{cat}^{-1} under UV and visible light irradiation, respectively. In addition, the results of the effects of the photocatalyst dosage and the gas phase-to-liquid phase volumetric ratio indicated that the hydrogen diffusability into the gas phase significantly affects the photocatalytic hydrogen production efficiency of the mesoporous-assembled $SrTiO_3$-based photocatalyst.

6.5 Acknowledgments

The Commission on Higher Education, Ministry of Education, Thailand, is acknowledged for providing a Ph.D. scholarship (a Project on Faculty Development in Shortage Area Scholarship) to the first author. This work was also supported by the Thailand Research Fund (TRF) and the Commission on Higher Education, Thailand; the Sustainable Petroleum and Petrochemicals Research Unit, Center for Petroleum, Petrochemicals, and Advanced Materials, Chulalongkorn University, Thailand; and the Petrochemical and Environmental Catalysis Research Unit, Ratchadapisek Somphot Endowment Fund, Chulalongkorn University, Thailand.

6.6 References

[1] A.L. Linsebigler, G. Lu, J.T. Yates, Photocatalysis on TiO_2 Surfaces: Principles, Mechanisms, and Selected Results, Chem. Rev. 95 (1995) 735-758.

[2] J.R. Bolton, Solar Photoproduction of Hydrogen: A Review, Sol. Energ. 57 (1996) 37-50.

[3] M. Ashokkumar, An Overview on Semiconductor Particulate Systems for Photoproduction of Hydrogen, Int. J. Hydrogen Energ. 23 (1998) 427-438.

[4] K. Sayama, H. Arakawa, Significant Effect of Carbonate Addition on Stoichiometric Photodecomposition of Liquid Water into Hydrogen and Oxygen from Platinum-Titanium(IV) Oxide Suspension, J. Chem. Soc.: Chem. Commun. 2 (1992) 150-152.

[5] K. Sayama, H. Arakawa, Effect of Na_2CO_3 Addition on Photocatalytic Secomposition of Liquid Water over Various Semiconductor Catalysis, J. Photochem. Photobiol. A: Chem. 77 (1994) 243-247.

[6] K. Sayama, H. Arakawa, Effect of Carbonate Addition on the Photocatalytic Decomposition of Liquid Water over a ZrO_2 Catalyst, J. Photochem. Photobiol. A: Chem. 94 (1996) 67-76.

[7] K. Sayama, H. Arakawa, Solar hydrogen production. Significant Effect of Na_2CO_3 Addition on Water Splitting Using Simple Oxide Semiconductor Photocatalysts, Catal. Surv. Jpn. 4 (2000) 75-80.

[8] R. Abe, K. Sayama, H. Arakawa, Significant Effect of Iodide Addition on Water Splitting into H_2 and O_2 over Pt-Loaded TiO_2 Photocatalyst: Suppression of Backward Reaction, Chem. Phys. Lett. 371 (2003) 360-364.

[9] Z. Zou, J. Ye, K. Sayama, H. Arakawa, Direct Splitting of Water under Visible Light Irradiation with an Oxide Semiconductor Photocatalyst, Nature 414 (2001) 625-627.

[10] R. Konta, T. Ishii, H. Kato, A. Kudo, Photocatalytic Activities of Noble Metal Ion Doped $SrTiO_3$ under Visible Light Irradiation, J. Phys. Chem. B 108 (2004) 8992-8995.

[11] A. Kudo, Development of Photocatalyst Materials for Water Splitting, Int. J. Hydrogen Energ. 31 (2006) 197-202.

[12] R. Dholam, N. Patel, M. Adami, A. Miotello, Physically and Chemically Synthesized TiO_2 Composite Thin Films for Hydrogen Production by Photocatalytic Water Splitting. Int. J. Hydrogen Energ. 33 (2008) 6896-6903.

[13] Z. Li, Y. Wang, J. Liu, G. Chen, Y. Li, C. Zhou, Photocatalytic Hydrogen Production from Aqueous Methanol Solutions under Visible Light over $Na(Bi_xTa_{1-x})O_3$ Solid-Solution. Int. J. Hydrogen Energ. 34 (2009) 147-152.

[14] C. Zhou, G. Chen, Y. Li, H. Zhang, J. Pei, Photocatalytic Activities of $Sr_2Ta_2O_7$ Nanosheets Synthesized by a Hydrothermal Method. Int. J. Hydrogen Energ. 34 (2009) 2113-2120.

[15] R. Sasikala, A. Shirole, V. Sudarsan, T. Sakuntala, C. Sudakar, R. Naik, S.R. Bharadwaj, Highly Dispersed Phase of SnO_2 on TiO_2 Nanoparticles Synthesized by Polyol-Mediated Route: Photocatalytic Activity for Hydrogen Generation. Int. J. Hydrogen Energ. 34 (2009) 3621-3630.

[16] Y. Huang, Y. Wei, L. Fan, M. Huang, J. Lin, J. Wu, Photocatalytic Activities of $HLaNb_2O_7$ Prepared by Polymerized Complex Method. Int. J. Hydrogen Energ. 34 (2009) 5318-5325.

[17] R. Dholam, N. Patel, M. Adami, A. Miotello, Hydrogen Production by Photocatalytic Water-Splitting Using Cr- or Fe-Doped TiO_2 Composite Thin Films Photocatalyst. Int. J. Hydrogen Energ. 34 (2009) 5337-5346.

[18] Y. Li, M. Guo, S. Peng, G. Lu, S. Li, Formation of Multilayer-Eosin Y-Sensitized TiO_2 via Fe^{3+} Coupling for Efficient Visible-Light Photocatalytic Hydrogen Evolution. Int. J. Hydrogen Energ. 34 (2009) 5629-5636.

[19] L. Wang, W. Wang, M. Shang, W. Yin, S. Sun, L. Zhang, Enhanced Photocatalytic Hydrogen Evolution under Visible Light over $Cd_{1-x}Zn_xS$ Solid Solution with Cubic Zinc Blend Phase. Int. J. Hydrogen Energ. 35 (2010) 19-25.

[20] Y.J. Zhang, L. Zhang, S. Li, Synthesis of Al-Substituted Mesoporous Silica Coupled with CdS Nanoparticles for Photocatalytic Generation of Hydrogen. Int. J. Hydrogen Energ. 35 (2010) 438-444.

[21] T. Sreethawong, S. Yoshikawa, Enhanced Photocatalytic Hydrogen Evolution over Pt Supported on Mesoporous TiO_2 Prepared by Single-Step Sol-Gel Process with Surfactant Template. Int. J. Hydrogen Energ. 31 (2006) 786-796.

[22] M. Ni, M.K.H. Leung, D.Y.C. Leung, K. Sumathy, A Review and Recent Developments in Photocatalytic Water-Splitting Using TiO_2 for Hydrogen Production. Renew. Sust. Energ. Rev. 11 (2007) 401-425.

[23] S. Chavadej, P. Phuaphromyod, E. Gulari, P. Rangsunvigit, T. Sreethawong, Photocatalytic Degradation of 2-Propanol by Using Pt/TiO_2 Prepared by Microemulsion Technique. Chem. Eng. J. 137 (2008) 489-495.

[24] H. Yi, T. Peng, D. Ke, D. Ke, L. Zan, C. Yan, Photocatalytic H_2 Production from Methanol Aqueous Solution over Titania Nanoparticles with Mesostructures. Int. J. Hydrogen Energ. 33 (2008) 672-678.

[25] W. Sun, S. Zhang, Z. Liu, C. Wang, Z. Mao, Studies on the Enhanced Photocatalytic Hydrogen Evolution over Pt/PEG-Modified TiO_2 Photocatalysts. Int. J. Hydrogen Energ. 33 (2008) 1112-1117.

[26] X. Fu, J. Long, X. Wang, D.Y.C. Leung, Z. Ding, L. Wu, Z. Zhang, Z. Li, X. Fu, Photocatalytic Reforming of Biomass: A Systematic Study of Hydrogen Evolution from Glucose Solution. Int. J. Hydrogen Energ. 33 (2008) 6484-6491.

[27] X.J. Zheng, L.F. Wei, Z.H. Zhang, Q.J. Jiang, Y.J. Wei, B. Xie, M.B. Wei, Research on Photocatalytic H_2 Production from Acetic Acid Solution by Pt/TiO_2 Nanoparticles under UV Irradiation. Int. J. Hydrogen Energ. 34 (2009) 9033-9041.

[28] M. Anpo, Preparation, Characterization, and Reactivities of Highly Functional Titanium Oxide-Based Photocatalysts Able to Operate under UV-Visible Light Irradiation: Approaches in Realizing High Efficiency in the Use of Visible Light. Bull. Chem. Soc. Jpn. 77 (2004) 1427-1442.

[29] T. Sreethawong, Y. Suzuki, S. Yoshikawa, Photocatalytic Evolution of Hydrogen over Mesoporous TiO_2 Supported NiO Photocatalyst Prepared by Single-Step Sol-Gel Process with Surfactant Template. Int. J. Hydrogen Energ. 30 (2005) 1053-1062.

[30] T. Sreethawong, S. Ngamsinlapasathian, Y. Suzuki, S. Yoshikawa, Nanocrystalline Mesoporous Ta_2O_5-Based Photocatalysts Prepared by Surfactant-Assisted Templating Sol-Gel Process for Photocatalytic H_2 Evolution. J. Mol. Catal. A: Chem. 235 (2005) 1-11.

[31] K. Domen, A. Kudo, T. Onishi, Mechanism of Photocatalytic Decomposition of Water into H_2 and O_2 over NiO-$SrTiO_3$. J. Catal. 102 (1986) 92-98.

[32] K. Sayama, K. Mukasa, R. Abe, Y. Abe, H. Arakawa, A New Photocatalytic Water Splitting System under Visible Light Irradiation Mimicking a Z-Scheme Mechanism in Photosynthesis. J. Photochem. Photobiol. A: Chem. 148 (2002) 71-77.

[33] A. Kudo, H. Kato, S. Nakagawa, Water Splitting into H_2 and O_2 on New $Sr_2M_2O_7$ (M = Nb and Ta) Photocatalysts with Layered Perovskite Structures: Factors Affecting the Photocatalytic Activity. J. Phys. Chem. B 104 (2000) 571-575.

[34] T. Puangpetch, T. Sreethawong, S. Yoshikawa, S. Chavadej, Synthesis and Photocatalytic Activity in Methyl Orange Degradation of Mesoporous-Assembled $SrTiO_3$ Nanocrystals Prepared by Sol-Gel Method with the Aid of Structure-Directing Surfactant. J. Mol. Catal. A: Chem. 287 (2008) 70-79.

[35] T. Puangpetch, T. Sreethawong, S. Yoshikawa, S. Chavadej, Hydrogen Production from Photocatalytic Water Splitting over Mesoporous-Assembled $SrTiO_3$ Nanocrystal-Based Photocatalysts. J. Mol. Catal. A: Chem. 312 (2009) 97-106.

[36] T. Ishii, H. Kato, A. Kudo, H_2 Evolution from an Aqueous Methanol Solution on $SrTiO_3$ Photocatalysts Codoped with Chromium and Tantalum Ions under Visible Light Irradiation. J. Photochem. Photobiol. A: Chem. 163 (2004) 181-186.

[37] V. Subramanian, R.K. Roeder, E.E. Wolf, Synthesis and UV-Visible-Light Photoactivity of Noble-Metal-$SrTiO_3$ Composites. Ind. Eng. Chem. Res. 45 (2006) 2187-2193.

[38] B.D. Cullity, Elements of X-ray Diffraction, Addison-Wesley Publishing Co., Reading, MA, 1978.

[39] P.V. Kamat, Handbook of Nanostructured Materials and Nanotechnology: Semiconductor Nanoparticles, Academic Press, New York, 1999, pp. 292-234.

[40] T. Sreethawong, S. Yoshikawa, Comparative Investigation on Photocatalytic Hydrogen Evolution over Cu-, Pd-, and Au-Loaded Mesoporous TiO_2 Photocatalysts. Catal. Commun. 6 (2005) 661-668.

[41] M. Moonsiri, P. Rangsunvigit, S. Chavadej, E. Gulari, Effects of Pt and Ag on the Photocatalytic Degradation of 4-Chlorophenol and Its By-Products. Chem. Eng. J. 97 (2004) 241-248.

[42] S. Pavasupree, Y. Suzuki, S. Pivsa-Art, S. Yoshikawa, Preparation and Characterization of Mesoporous TiO_2-CeO_2 Nanopowders Respond to Visible Wavelength. J. Solid State Chem. 178 (2005) 128-134.

[43] T. Sreethawong, S. Chavadej, Color Removal of Distillery Wastewater by Ozonation in the Absence and Presence of Immobilized Iron Oxide Catalyst. J. Hazard. Mater. 155 (2008) 486-493.

[44] A.D. McNaught, A. Wilkinson, IUPAC Compendium of Chemical Terminology, Second ed., Cambridge, UK, 1997.

[45] Kenneth Barbalace Periodic Table of Elements, Envionmentalchemistry.com. 1995-2009. Available at: http://Environmentalchemistry.com (Retrieved on September 23, 2009)

[46] R.A. Evarestov, A.V. Bandura, V.E. Alexandrov, Adsorption of Water on (001) Surface of $SrTiO_3$ and $SrZrO_3$ Cubic Perovskites: Hybrid HF-DFT LCAO Calculations. Surf. Sci. 601 (2007) 1844-1856.

[47] S. Ikeda, K. Hirao, S. Ishino, M. Matsumura, B. Ohtani, Preparation of Platinized Strontium Titanate Covered with Hollow Silica and Its Activity for Overall Water Splitting in a Novel Phase-Boundary Photocatalytic System. Catal. Today 117 (2006) 343-349.